Hindawi Publishing Corporation
International Journal of Photoenergy
Volume 2014, Article ID 580615, 7 pages
http://dx.doi.org/10.1155/2014/580615

Research Article

Solvothermal Synthesis of Zn_2SnO_4 Nanocrystals and Their Photocatalytic Properties

Guang Sun, Saisai Zhang, and Yanwei Li

Cultivating Base for Key Laboratory of Environment-Friendly Inorganic Materials in University of Henan Province, School of Materials Science and Engineering, Henan Polytechnic University, Jiaozuo, Henan 454000, China

Correspondence should be addressed to Guang Sun; mcsunguang@163.com

Received 22 January 2014; Revised 16 February 2014; Accepted 17 February 2014; Published 23 March 2014

Academic Editor: Lei Liu

Crystalline Zn_2SnO_4 nanoparticles were successfully synthesized via a simple solvothermal route by using $Zn(CH_3COO)_2{\cdot}2H_2O$ and $SnCl_4{\cdot}5H_2O$ as source materials, NaOH as mineralizing agent, and water and ethanol as mixed solvents. The used amount of NaOH was found to have an important influence on the formation of Zn_2SnO_4. When the molar ratio of $OH^- : Zn^{2+} : Sn^{4+}$ was set in the range from 4 : 2 : 1 to 8 : 2 : 1, Zn_2SnO_4 nanoparticles with different shape and size were obtained. However, when the molar ratio of $OH^- : Zn^{2+} : Sn^{4+}$ was set as 10 : 2 : 1, a mixture phase of ZnO and $ZnSn(OH)_6$ instead of Zn_2SnO_4 was obtained. Photodegradation measurements indicated that the Zn_2SnO_4 nanoparticles own better photocatalytic property to depredate methyl orange than the Zn_2SnO_4 nanopolyhedrons. The superior photocatalytic properties of Zn_2SnO_4 nanoparticles may be contributed to their small crystal size and high surface area.

1. Introduction

In recent years, metal oxide semiconductors (MOSs) have been paid more and more attentions due to their diverse function and promising application in various fields. Among these MOSs, besides the widely studied binary oxides such as ZnO [1], SnO_2 [2], TiO_2 [3], and Fe_2O_3 [4], the ternary MOSs, including Zn_2SnO_4 and $ZnSnO_3$, have also been investigated [5, 6]. Stimulated by the prominent morphology (shape and size) dependent physical and chemical properties of nanostructured MOS, many researchers have devoted their efforts to the design and synthesis of MOS nanostructures. Up to now, a variety of nanostructures, such as zero-dimensional nanoparticles, one-dimensional nanowires, nanorods and nanotubes, two-dimensional nanosheets, and three-dimensional hierarchical micro/nanostructures that assembled with low dimensional nanobuilding blocks, have been synthesized and investigated. However, it is still a meaningful and important work to develop facile and feasible techniques for the synthesis of MOS nanomaterials with controlled shape and size in the field of nanoscience and nanotechnology.

Zn_2SnO_4, as an important ternary MOS, is a typical n-type semiconductor with the band-gap of 3.6 eV. Because of its high chemical sensitivity, low visible absorption, and excellent optical electronic properties, Zn_2SnO_4 has many promising applications in gas sensors [5, 7, 8], solar cells [9, 10], photocatalysts [11–15], and negative materials for rechargeable lithium ion batteries [16, 17]. Driven by these potential applications, an increasing research interest has focused on the synthesis of Zn_2SnO_4. In order to achieve Zn_2SnO_4, some traditional high-temperature techniques are usually employed, including high-temperature solid-reaction between solid ZnO and SnO_2 [18, 19], thermal evaporation method by heating metal or metal oxides at high temperature [20–23], and the chemical vapor deposition methods [24]. However, these reported methods are usually of high energy consumption, and thus not suitable for practical production in industry from the view point of environment protection. Recently, hydrothermal synthesis methods have been successfully developed to prepare Zn_2SnO_4 [5, 11, 25–29]. Compared with the high-temperature synthesis methods mentioned above, the hydrothermal synthesis method has the merits of low cost and being friendly to environment and is thus considered as one of the most promising methods that can be applied in practical production. Up to now, various micro/nanostructures of Zn_2SnO_4 have been synthesized

by hydrothermal methods, such as nanowires [23, 24, 29], nanorods [28], irregular particles [17], well-defined polyhedra [22, 30], and hierarchical cube-like microstructures assembled with nanoplates [8]. As an evolution method of hydrothermal synthesis, the solvothermal synthesis is also an important wet chemical synthesis method that can be used to fabricate MOS nanostructures. However, compared with the widely reported hydrothermal synthesis methods for Zn_2SnO_4, few reports are about the synthesis of Zn_2SnO_4 nanostructure via solvothermal method.

In this paper, a simple and efficient solvothermal route was developed to synthesize crystalline Zn_2SnO_4 nanoparticles by using water and ethanol as mixed solvents. The prepared samples were characterized by X-ray diffraction (XRD), transmission electron microscopy (TEM), Fourier infrared spectroscopy (FTIR), and nitrogen-sorption techniques. It was found that the crystallinity, particle size, and shape of Zn_2SnO_4 are strongly dependent on the amount of alkali. The photocatalytic properties of the prepared Zn_2SnO_4 were investigated by photodegradation of methyl orange dye. Results indicated that the irregular Zn_2SnO_4 nanoparticles own better photodegradation capacity than Zn_2SnO_4 nanopolyhedrons perhaps due to their smaller crystal size and higher surface area.

2. Experimental Section

2.1. Synthesis of the Zn_2SnO_4. All of the chemical reagents were analytical grade and used as received without further purification. In this paper, Zn_2SnO_4 was prepared via a simple solvothermal method by using $Zn(CH_3COO)_2{\cdot}2H_2O$ and $SnCl_4{\cdot}5H_2O$ as starting materials, NaOH as mineralizing agent, and distilled water and absolute ethanol as mixed solvents. In a typical experiment for synthesizing Zn_2SnO_4, the molar ratio of $OH^- : Zn^{2+} : Sn^{4+}$ was set as 6 : 2 : 1. In detail, 0.525 g $SnCl_4{\cdot}5H_2O$ and 0.659 g $Zn(CH_3COO)_2{\cdot}2H_2O$ were dissolved in 20 mL ethanol under magnetic stirring, followed by dropping 20 mL aqueous solution of NaOH (0.45 M). After stirring for 30 min, the obtained white slurry was transferred to a 50 mL Teflon-lined autoclave and then maintained at 160°C for 24 h. When the autoclave was cooled down to room temperature naturally, the white precipitates were collected by centrifugation, washed several times with absolute ethanol and distilled water, and finally dried at 80°C in air for 5 h to get the final products. For comparison, parallel experiments were also carried out by varying the molar ratio of $OH^- : Zn^{2+} : Sn^{4+}$. The samples prepared at the molar ratio of $OH^- : Zn^{2+} : Sn^{4+}$ of 4 : 2 : 1, 6 : 2 : 1, 8 : 2 : 1 and 10 : 2 : 1 were denoted as 4S, 6S, 8S, and 10S, respectively.

2.2. Characterization. The phase structure and purity of the as-prepared products were characterized by powder X-ray diffraction (XRD) on Bruker D8 diffractometer with Cu Kα radiation (λ = 1.54056 nm). The transmission electron microscopy (TEM) images, selected area electron diffraction (SAED) patterns, and high resolution TEM (HRTEM) images were collected on a JEM-2100 TEM. N_2 adsorption-desorption isotherms were collected at liquid nitrogen temperature using Quantachrome AsiQM0000-3 sorption analyzer. The specific surface area was calculated using multipoint Brunauer-Emmett-Teller (BET) method. The pore size distribution was determined from the adsorption branch of the isotherms using the DFT method. Before carrying out the measurement, each sample was degassed at 180°C for more than 6 h.

2.3. Measurement of Photocatalytic Activities. The photocatalytic activities of the as-prepared Zn_2SnO_4 were measured by photodegradation of methyl orange (MO) at room temperature. In a typical experiment, 50 mg as-prepared catalyst was suspended in 100 mL MO aqueous solutions (20 mg/L) in a water-jacketed reactor with the capacity of 200 mL. The UV lamp (TUV 4W/G4 T5, Philips, wavelength 254 nm) was placed above the reactor, and the distance between the lamp and liquid level was 10 cm. Before UV-light irradiation, the suspensions were stirred in dark for 30 min to ensure the establishment of absorption-desorption equilibrium. During the experiment, 3 mL reaction solution was taken out from the reaction system at a certain time interval and then centrifuged to remove the solid catalyst. After that, the obtained MO solution was analyzed on a UV-Vis spectrophotometer (TU-1810) in the wavelength range of 200–700 nm.

3. Results and Discussion

3.1. Characterization of the Prepared Samples

3.1.1. XRD Analysis. The phase structure and purity of the prepared samples was analyzed by XRD. Figure 1 shows the typical XRD patterns of the samples prepared at different conditions. It can be seen that when the molar ratio of $OH^- : Zn^{2+} : Sn^{4+}$ was in the range of 4 : 2 : 1–8 : 2 : 1, cubic inverse spinal Zn_2SnO_4 phases can be successfully obtained. For example, as shown in Figure 1 (c), all the appeared reflection peaks from low angle area to high angle area can be indexed as perfect cubic inverse spinal Zn_2SnO_4 (JCPDS no. 24-1470). In the XRD patterns of 4S, 6S, and 8S (Figure 1 (a) to (c), resp.), no peaks from other crystal phases are detected, such as ZnO and SnO_2. This result indicates that the samples prepared at present condition are of pure Zn_2SnO_4 phase. Compared with 8S, the refection peaks of 4S and 6S are seriously broaden, which suggested that the used amount of alkali has important influences on the crystallinity of Zn_2SnO_4. In contrast, when the molar ratio of $OH^- : Zn^{2+} : Sn^{4+}$ was increased to 10 : 2 : 1, as shown, the XRD pattern of 10S in Figure 1 (d), two crystalline phases of cubic $ZnSn(OH)_6$ (JCPDS file no. 20-1455), and hexagonal ZnO (JCPDS file no. 36-1451) are observed, which indicates that a mixture of $ZnSn(OH)_6$ and ZnO is obtained instead of the single Zn_2SnO_4 phase. Such result may be attributed to using excessive amount of alkali.

3.1.2. FT-IR Analysis. The chemical-bond types of the prepared Zn_2SnO_4 were investigated by FT-IR. Figure 2 shows the typical FT-IR spectra of the prepared 4S, 6S, and 8S. From the FT-IR spectra, we can see that the three samples exhibit similar characteristics of infrared adsorption bands, which are quite similar to the spinal Zn_2SnO_4 reported in previous

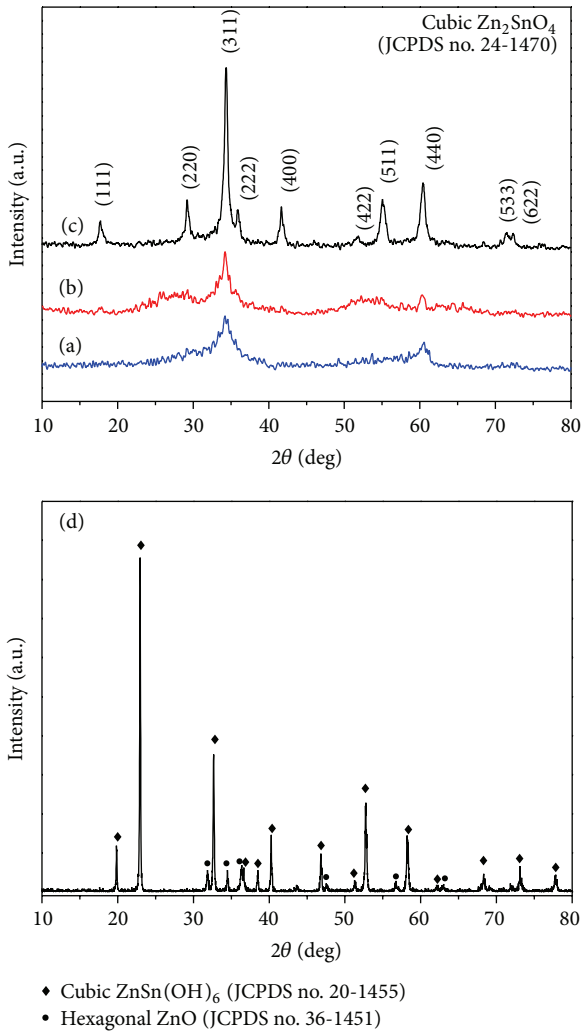

Figure 1: XRD patterns of the prepared samples (a) 4S, (b) 6S, (c) 8S, and (d) 10S.

literatures [11, 31]. Therein, the broad absorption peaks at 3426 and 1602 cm^{-1} can be ascribed to the vibration of absorptive water, and the absorption peaks at 546, 1038, and 1410 cm^{-1} are due to the vibration of M–O or M–O–M groups in Zn_2SnO_4. The results given by FT-IR analysis further confirm the formation of Zn_2SnO_4 and thus corroborate the results obtained in XRD analysis.

3.1.3. TEM Analysis. In order to obtain the detailed structural information of the as-prepared Zn_2SnO_4, further measurements by TEM and HR-TEM were performed. Figures 3(a)–3(c) show the typical TEM images of the prepared Zn_2SnO_4 samples. From Figures 3(a) and 3(b), it can be seen that a large scale of nanosized particles with irregular shapes are obtained in 4S and 6S, respectively. The size of these nanoparticles is measured to be about 5–8 nm for 4s and 12–15 nm for 6S. In order to minimize their surface energy, most of these formed nanoparticles aggregated together loosely. As for 8S, besides the irregular nanoparticles, many polyhedron-like particles with the size about 30 nm are also

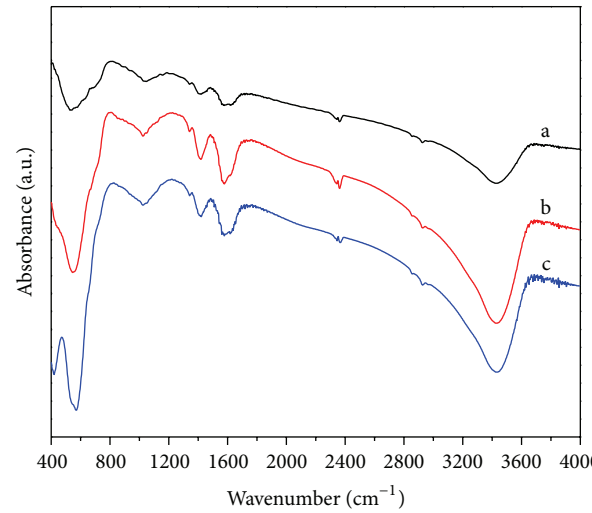

Figure 2: FT-IR spectra of (a) 4S, (b) 6S, and (c) 8S.

formed (Figure 3(c)), being obviously different from that observed in 6S and 8S. The different crystallite size and shape in the obtained Zn_2SnO_4 samples indicated that the used amount of alkali may have important influence on the formation of Zn_2SnO_4. Relatively high concentration of NaOH is favorable for achieving Zn_2SnO_4 with larger size. Moreover, it is worthy to be mentioned that in the three samples numerous nanopores with different size were formed in the interspaces among the nanoparticles due to their loosely aggregated characteristics, as shown in Figures 1 (a), (b), and (c). The existence of porous structure in the prepared Zn_2SnO_4 samples can be further convinced by following N_2-sorption analysis. The insets in Figures 3(a)–3(c) show the corresponding selected area electron diffraction (SAED) images of 4S, 6S, and 8S, respectively. The appeared diffraction rings in the SAED patterns demonstrate the polycrystalline nature of the prepared Zn_2SnO_4 samples. Figure 3(d) displays a representative HR-TEM image taken from one of the observed Zn_2SnO_4 nanoparticles in Figure 3(b). The distance between the adjacent lattice fringes is measured to be 0.263 nm, which can be attributed to the (311) crystal plane of cubic inverse spinal Zn_2SnO_4 (JCPDS no. 24-1470). This result is consistent with the XRD analysis, which further proved the preparation of crystalline Zn_2SnO_4 by the present solvothermal method.

3.1.4. N_2-Sorption Analysis. N_2-sorption measurements were further performed on the prepared Zn_2SnO_4 samples to obtain the information of specific surface area and pore structure. Figure 4 depicts the nitrogen adsorption-desorption isotherms and the corresponding pore size distributions of 4S, 6S, and 8S. From Figure 4(a) it can be seen that the adsorption-desorption isotherms of all three samples exhibit a type of IV-like behavior including a type H3 hysteresis loop according to the IUPAC classification. Such result demonstrated the existence of mesoporous structure in the prepared samples, which is in agreement with the TEM

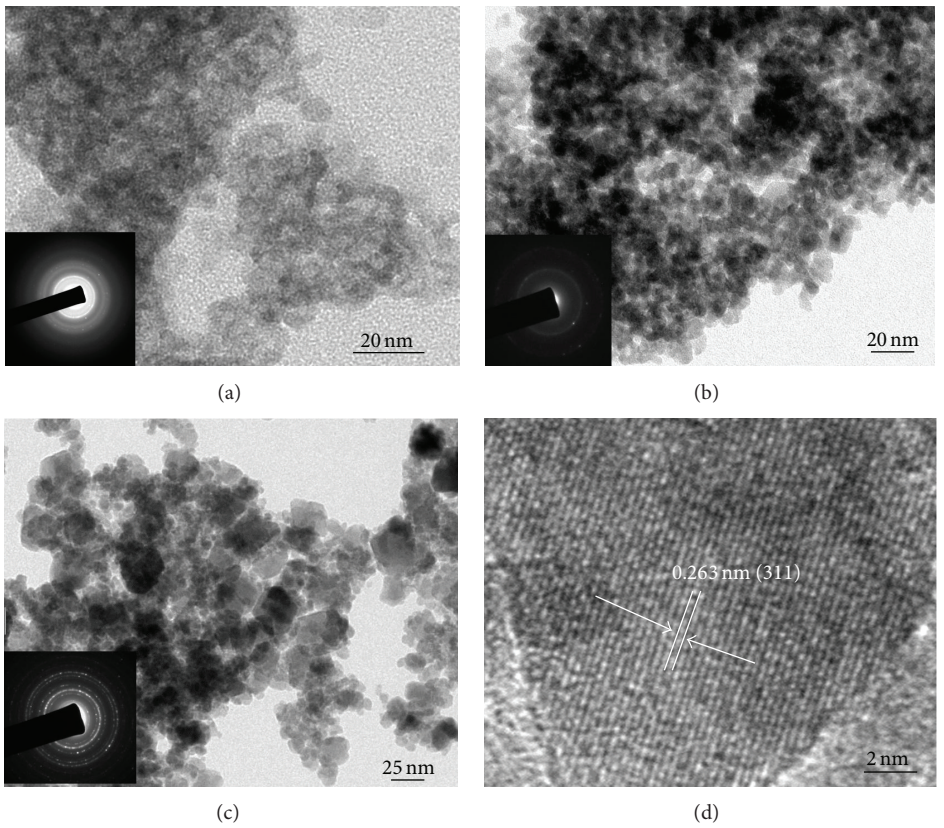

Figure 3: TEM images of (a) 4S, (b) 6S, and (c) 8S and (d) the HR-TEM image corresponding to (c). The SAED patterns are shown as an inset in corresponding TEM images.

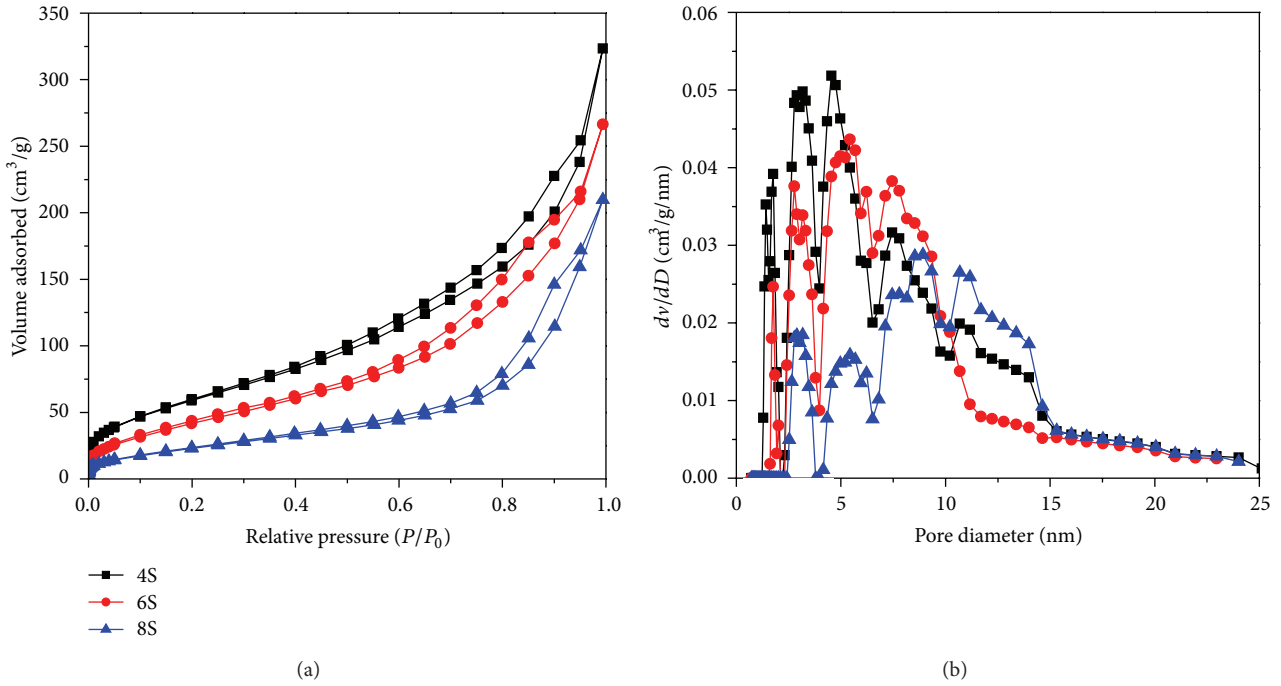

Figure 4: (a) N_2 adsorption-desorption isotherms and (b) the corresponding pore size distribution curves of 4S, 6S, and 8S.

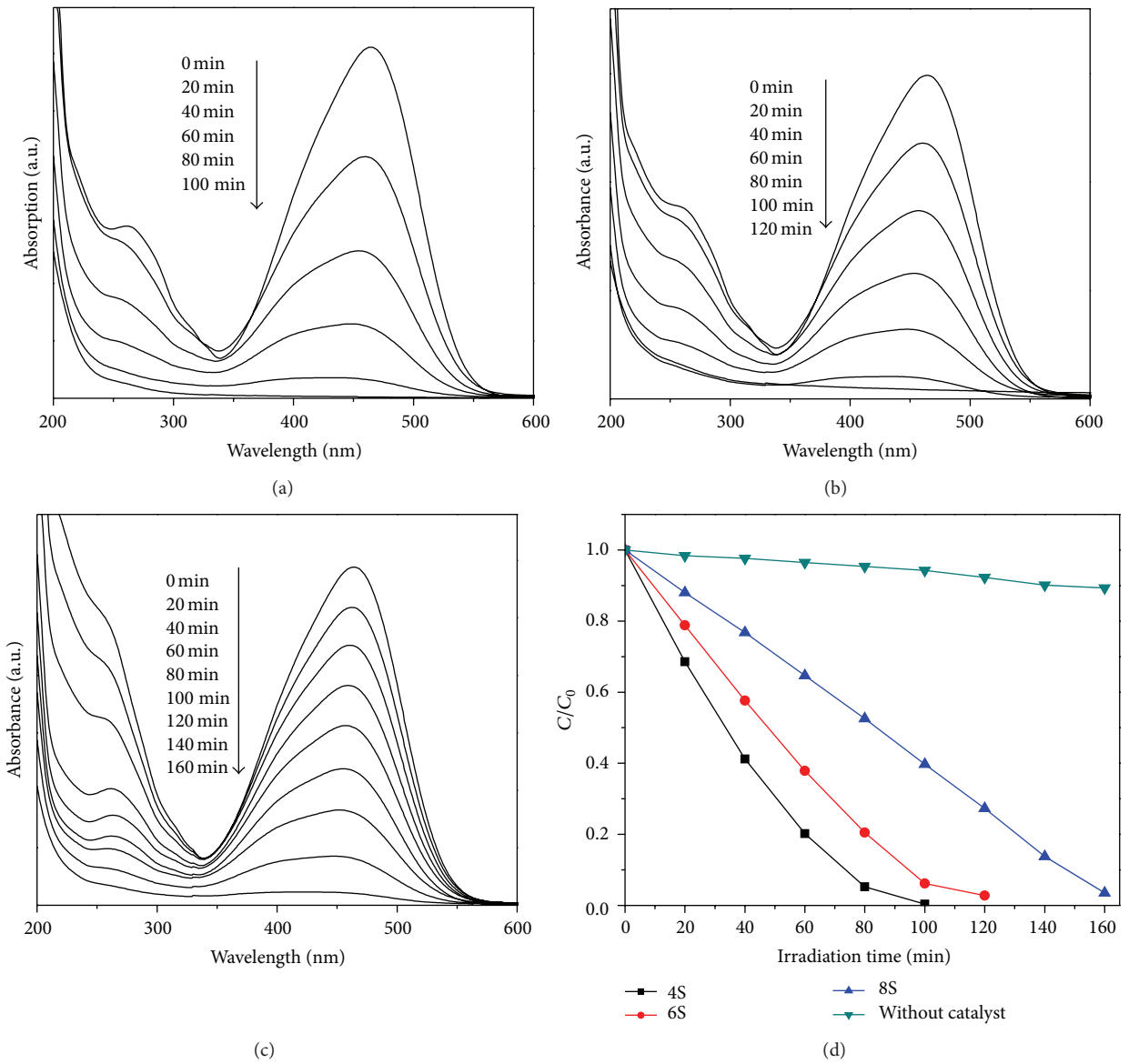

Figure 5: Temporal evolution of MO absorption spectra under irradiation of UV-light by using as-prepared Zn_2SnO_4 as photocatalyst: (a) 4S, (b) 6S, and (c) 8S; (d) photodegradation of MO as a function of irradiation time, in which C is the concentration of MO and C_0 is the initial concentration.

observation. The pore size distribution curves (Figure 4(b)) of the prepared Zn_2SnO_4 samples, being estimated based on the DFT method from the adsorption branch of the isotherm, indicated that the pore size distribution range for 4S and 6S was mainly centered at 1.7–10 nm, which was smaller than that of 8S (3–14.5 nm). As for the three Zn_2SnO_4 samples, the relative wide pore-size distribution may be mainly contributed to the random and disordered aggregation characteristics of Zn_2SnO_4 nanocrystals in the products. The calculated BET surface areas for 4S, 6S, and 8S were found to be 226, 166, and 91 $m^2 \cdot g^{-1}$, respectively. Obviously, the surface area of 4S and 6S was higher than that of 8S. Combined with the TEM analysis, it can be concluded that the surface area of the prepared samples seriously decreased with the increasing of crystal size of Zn_2SnO_4.

3.2. Photocatalytic Properties Studies. In general, the photocatalytic properties of MOS can be influenced by many factors, such as the crystal size, exposed crystal plane, morphology, and band structure. In terms of our experiment, the crystal size and the surface area of Zn_2SnO_4 can be controlled by adjusting the used amount of alkali in the reaction system. Therefore, it was expected that the Zn_2SnO_4 samples prepared under different conditions can bring different photocatalytic activities. So, in order to evaluate the photocatalytic activity of the prepared Zn_2SnO_4, the experiments of photodegradation of methyl orange (MO) were performed under UV-light irradiation. Figures 5(a)–5(c) show the time-dependent absorption spectra of MO solution containing different Zn_2SnO_4 catalysts during the UV-light irradiation. It can be seen that the characteristic absorption

peak of MO centered around 465 nm decreased rapidly in intensity with the irradiation time and almost disappeared after undergoing a certain time of irradiation. The decreased speed of MO concentration in Figures 5(a) and 5(b) was found to be faster than that in Figure 5(c), indicating that the photodegradation capacity of 4S and 6S is stronger than that of 8S. The photodegradation plots of MO under UV-light by using different Zn_2SnO_4 samples as catalysts are shown in Figure 5(d), in which A_0/A was substituted by C_0/C, where C_0 and C are the initial and actual concentration of MO, respectively, because the normalized concentration of the solution equals the normalized maximum absorbance. For comparison, the degradation plot of MO without any catalyst is also displayed in Figure 5(d). It can be seen that when there was no catalyst in the reaction system, the decrease of C_0/C is very slow and almost negligible. After irradiating for 100 min, only about 0.5% of total MO molecules were depredated. However, once the catalyst of Zn_2SnO_4 was added, a rapid decrease of C/C_0 was observed, indicating that the prepared Zn_2SnO_4 samples are effective to depredate MO molecules. Under the same irradiation period, the values of C_0/C for 4S and 6S were larger than thos for 8S, indicating their better photocatalytic activity than 8S. After 100 min irradiation, the C_0/C values for 4S, 6S, and 8S are about 0, 0.06, and 0.6, corresponding to the degradation about 100%, 96%, and 40% of total MO molecules, respectively. The superior photocatalytic activity of 4S and 6S can be explained by their smaller crystal size and larger surface area. It is generally accepted that the catalytic process is mainly related to the adsorption and desorption of organic dye molecules on the surface of the catalyst. The higher specific surface area of 4S ($226\,m^2 \cdot g^{-1}$) and 6S ($166\,m^2 \cdot g^{-1}$) can provide more unsaturated surface coordination sites exposed to the solution and more opportunities for dye molecules to absorb on the surface of catalysts, resulting in the production of more active reaction sites. Moreover, the mesoporous structures in the catalysts enable storage of more dye molecules, which can also promote the photocatalytic properties. Furthermore, the bandgap of the catalyst material may be another important factor that can influence the photocatalytic properties. In our experiment, the crystallite size of Zn_2SnO_4 in 4S and 6S was observed to be less than 20 nm. Therefore, the bandgap of Zn_2SnO_4 catalyst may be broadened by the quantum size effect. The broadened bandgap can not only bring higher redox potentials but also promote electrons transferring form the conductive band of Zn_2SnO_4 with high electric potential to those with low electric potential. Thus, the recombination of the photogenerated electron-hole pair can be hampered, which in turn results in the enhancement of the charge-transfer rates in the catalyst.

4. Conclusions

In summary, a simple solvothermal route was successfully developed for controlled synthesis of Zn_2SnO_4 nanocrystals with different shape and size. Irregular Zn_2SnO_4 nanoparticles about 5–8 nm (4S) and 12–15 nm in size (6S) and polyhedron-like Zn_2SnO_4 nanoparticles about 30 nm in size (8S) can be easily obtained by adjusting the used amount of alkali. The BET surface areas of the prepared samples of 4S, 6S, and 8S were measured to be 226, 166, and $91\,m^2 \cdot g^{-1}$, respectively. Due to the higher specific surface area and quantum size effects, the 4S and 6S exhibited higher photocatalytic activity to degrade MO than 8S.

Conflict of Interests

The authors have no conflict of interests in relation to the instrumental companies directly or indirectly.

Acknowledgments

This work was supported by the National Natural Science Foundation of China (51172065), Program for Innovative Research Team in the University of Henan Province (2012IRTSTHN007), Foundation of Henan Scientific and Technology Key Project (112102310425, 112102310029, and 132102210251), the Education Department Natural Science Foundation of Henan Province (2011B150009 and 13A430315), China Postdoctoral Science Foundation funded project (2012M521394), and Specialized Research Fund for the Doctoral Program of Higher Education (20124116120002).

References

[1] D.-F. Zhang, L.-D. Sun, J.-L. Yin, C.-H. Yan, and R.-M. Wang, "Attachment-driven morphology evolvement of rectangular ZnO nanowires," *Journal of Physical Chemistry B*, vol. 109, no. 18, pp. 8786–8790, 2005.

[2] C. Wang, G. H. Du, K. Ståhl, H. X. Huang, Y. J. Zhong, and J. Z. Jiang, "Ultrathin SnO_2 nanosheets: oriented attachment mechanism, nonstoichiometric defects, and enhanced lithium-ion battery performances," *Journal of Physical Chemistry C*, vol. 116, no. 6, pp. 4000–4011, 2012.

[3] X. C. Ma, Y. Dai, M. Guo, and B. B. Huang, "Relative photooxidation and photoreduction activities of the 100, 101, and 001 surfaces of Anatase TiO_2," *Langmuir*, vol. 29, no. 44, pp. 13647–13654, 2013.

[4] X. D. Xu, R. G. Cao, S. Y. Jeong, and J. Cho, "Spindle-like mesoporous α-Fe_2O_3 anode material prepared from MOF template for high-rate Lithium batteries," *Nano Letters*, vol. 12, no. 9, pp. 4988–4991, 2012.

[5] Y.-Q. Jiang, X.-X. Chen, R. Sun, Z. Xiong, and L.-S. Zheng, "Hydrothermal syntheses and gas sensing properties of cubic and quasi-cubic Zn_2SnO_4," *Materials Chemistry and Physics*, vol. 129, no. 1-2, pp. 53–61, 2011.

[6] J. R. Huang, X. J. Xu, C. P. Gu et al., "Size-controlled synthesis of porous $ZnSnO_3$ cubes and their gas-sensing and photocatalysis properties," *Sensors and Actuators B*, vol. 171-172, pp. 572–579, 2012.

[7] Z. Chen, M. H. Cao, and C. W. Hu, "Novel Zn_2SnO_4 hierarchical nanostructures and their gas sensing properties toward ethanol," *Journal of Physical Chemistry C*, vol. 115, no. 13, pp. 5522–5529, 2011.

[8] Y. Q. Jiang, C. X. He, R. Sun, Z. X. Xie, and L. S. Zheng, "Synthesis of Zn_2SnO_4 nanoplate-built hierarchical cube-like structures with enhanced gas-sensing properties," *Materials Chemistry and Physics*, vol. 136, pp. 689–704, 2012.

[9] B. Tan, E. Toman, Y. G. Li, and Y. Y. Wu, "Zinc stannate (Zn_2SnO_4) dye-sensitized solar cells," *Journal of the American Chemical Society*, vol. 129, no. 14, pp. 4162–4163, 2007.

[10] J. J. Chen, L. Y. Lu, and W. Y. Wang, "Zn_2SnO_4 nanowires as photoanode dye-sensitized solar cells and improvement on open-circuit voltage," *The Journal of Physical Chemistry C*, vol. 116, no. 20, pp. 10841–10847, 2012.

[11] J. Zeng, M. D. Xin, K. W. Li, H. Wang, H. Yan, and W. J. Zhang, "Transformation process and photocatalytic activities of hydrothermally synthesized Zn_2SnO_4 nanocrystals," *Journal of Physical Chemistry C*, vol. 112, no. 11, pp. 4159–4167, 2008.

[12] M. A. Alpuche-Aviles and Y. Wu, "Photoelectrochemical study of the band structure of Zn_2SnO_4 prepared by the hydrothermal method," *Journal of the American Chemical Society*, vol. 131, no. 9, pp. 3216–3224, 2009.

[13] Z. Ai, S. Lee, Y. Huang, W. Ho, and L. Zhang, "Photocatalytic removal of NO and HCHO over nanocrystalline Zn_2SnO_4 microcubes for indoor air purification," *Journal of Hazardous Materials*, vol. 179, no. 1–3, pp. 141–150, 2010.

[14] Z. Tian, C. Liang, J. Liu, H. Zhang, and L. Zhang, "Zinc stannate nanocubes and nanourchins with high photocatalytic activity formethyl orange and 2, 5-DCP degradation," *Journal of Materials Chemistry*, vol. 22, no. 33, pp. 17210–17214, 2012.

[15] T. K. Jia, J. W. Zhao, F. Fu et al., "Synthesis, characterization, and photocatalytic activity of Zn-Doped SnO_2/Zn_2SnO_4 coupled nanocomposites," *International Journal of Photoenergy*, vol. 2012, Article ID 198497, 6 pages, 2012.

[16] N. Feng, S. L. Peng, X. L. Sun et al., "Synthesis of monodisperse single crystal Zn_2SnO_4 cubes with high lithium storage capacity," *Materials Letters*, vol. 76, pp. 66–68, 2012.

[17] A. Rong, X. P. Gao, G. R. Li et al., "Hydrothermal synthesis of Zn_2SnO_4 as anode materials for Li-ion battery," *Journal of Physical Chemistry B*, vol. 110, no. 30, pp. 14754–14760, 2006.

[18] T. Hashemi, H. M. Al-Allak, J. Illingsworth, A. W. Brinkman, and J. Woods, "Sintering behaviour of zinc stannate," *Journal of Materials Science Letters*, vol. 9, no. 7, pp. 776–778, 1990.

[19] G. B. Palmer, K. R. Poeppelmeier, and T. O. Mason, "$Zn_{2-x}Sn_{1-x}In_{2x}O_{4-\delta}$: an indium-substituted spinel with transparent conducting properties," *Journal of Solid State Chemistry*, vol. 134, no. 1, pp. 192–197, 1997.

[20] J. S. Jie, G. Z. Wang, X. H. Han et al., "Growth of ternary oxide nanowires by gold-catalyzed vapor-phase evaporation," *Journal of Physical Chemistry B*, vol. 108, no. 24, pp. 8249–8253, 2004.

[21] H. Y. Chen, J. X. Wang, H. C. Yu, H. X. Yang, S. S. Xie, and J. Q. Li, "Transmission electron microscopy study of pseudoperiodically twinned Zn_2SnO_4 nanowires," *Journal of Physical Chemistry B*, vol. 109, no. 7, pp. 2573–2577, 2005.

[22] J.-W. Zhao, L.-R. Qin, and L.-D. Zhang, "Single-crystalline Zn_2SnO_4 hexangular microprisms: fabrication, characterization and optical properties," *Solid State Communications*, vol. 141, no. 12, pp. 663–666, 2007.

[23] Y. X. Du and P. Ding, "Thermal evaporation route to zinc stannate nanowires and the cathodoluminescence of the individual nanowires," *Journal of Alloys and Compounds*, vol. 502, no. 1, pp. L14–L16, 2010.

[24] Q. R. Hu, P. Jiang, H. Xu et al., "Synthesis and photoluminescence of Zn_2SnO_4 nanowires," *Journal of Alloys and Compounds*, vol. 484, no. 1-2, pp. 25–27, 2009.

[25] X. Lou, X. Jia, J. Xu, S. Liu, and Q. Gao, "Hydrothermal synthesis, characterization and photocatalytic properties of Zn_2SnO_4 nanocrystal," *Materials Science and Engineering A*, vol. 432, no. 1-2, pp. 221–225, 2006.

[26] S. Baruah and J. Dutta, "Zinc stannate nanostructures: hydrothermal synthesis," *Science and Technology of Advanced Materials*, vol. 12, no. 1, Article ID 013004, 2011.

[27] J. Fang, A. H. Huang, P. X. Zhu et al., "Hydrothermal preparation and characterization of Zn_2SnO_4 particles," *Materials Research Bulletin*, vol. 36, no. 7-8, pp. 1391–1397, 2001.

[28] H. L. Zhu, D. R. Yang, G. X. Yu, H. Zhang, D. L. Jin, and K. H. Yao, "Hydrothermal synthesis of Zn_2SnO_4 nanorods in the diameter regime of sub-5 nm and their properties," *Journal of Physical Chemistry B*, vol. 110, no. 15, pp. 7631–7634, 2006.

[29] L. S. Wang, X. Z. Zhang, X. Liao, and W. G. Yang, "A simple method to synthesize single-crystalline Zn_2SnO_4 (ZTO) nanowires and their photoluminescence properties," *Nanotechnology*, vol. 16, no. 12, pp. 2928–2931, 2005.

[30] M. Miyauchi, Z. Liu, Z.-G. Zhao, S. Anandan, and K. Hara, "Single crystalline zinc stannate nanoparticles for efficient photoelectrochemical devices," *Chemical Communications*, vol. 46, no. 9, pp. 1529–1531, 2010.

[31] C. G. Anchieta, D. Sallet, E. L. Foletto, S. S. Da Silva, O. Chiavone-Filho, and C. A. O. do Nascimento, "Synthesis of ternary zinc spinel oxides and their application in the photoderadation of organic pollutant," *Ceramicas International*, vol. 40, no. 3, pp. 4173–4178, 2014.